ELSEVIER

22 January 1996

PHYSICS LETTERS A

Physics Letters A 210 (1996) 382–390

On the behavior of the cathodically polarized Pd/D system: Search for emanating radiation

S. Szpak [a], P.A. Mosier-Boss [a,*,1], J.J. Smith [b]

[a] *Naval Command, Control and Ocean Surveillence Center RDT & E Division, San Diego, CA 92152-5000, USA*

[b] *Department of Energy, Washington, DC 20585, USA*

Received 14 November 1994; revised manuscript received 12 September 1995; accepted for publication 12 November 1995
Communicated by J.P. Vigier

Abstract

Evidence for the emission of low intensity X-rays during cathodic polarization of the Pd/D system(s) is presented. The Pd/D system was prepared by charging with electrochemically generated deuterium either palladium foil or palladium electrodeposited from D_2O electrolytes. Experimental and analytical procedures are described in detail.

1. Introduction

Production of excess energy in a cathodically polarized Pd/D system has been reported by Fleischmann and Pons [1]. In particular, they claimed that the rate of excess enthalpy generation could only be explained by a nuclear process since the magnitude of this excess was at least 100 times that of any known chemical reaction. However, the difficulty in accepting this view has been the lack of correlation between the excess energy produced and the quantity of nuclear debris generated by classical nuclear paths. Alternative models have been proposed which predict, irrespective of the origin of the source of excess heat production, that the requisite energy deposited within the Pd lattice should result in emanation of X-rays arising from the disturbance of the electronic structure of the Pd/D system [2–5].

In this Letter, we present data collected during an investigation of the emanation of soft X- and γ-rays in the course of the Pd/D codeposition and during the period of deuterium evolution on such electrodes reported by us previously [6]. In support of our conclusions, we provide detailed information on cell design, data collection and examine the statistics of background radiation measured for a period of months. In the interpretation of the X-ray data we include computer synthesis of events that tend to reproduce the experimentally observed spectra. Because of the lack of theoretical guidance, we present the experimental evidence and avoid interpretation of the mechanism(s) giving rise to the radiation.

2. Experimental

In developing the experimental procedure we have concentrated on the importance of shielding, sensitivity of detectors, and cell design.

* Corresponding author.
[1] E-mail: bossp@nosc.mil.

0375-9601/96/$12.00 © 1996 Elsevier Science B.V. All rights reserved
SSDI 0375-9601(95)00915-9

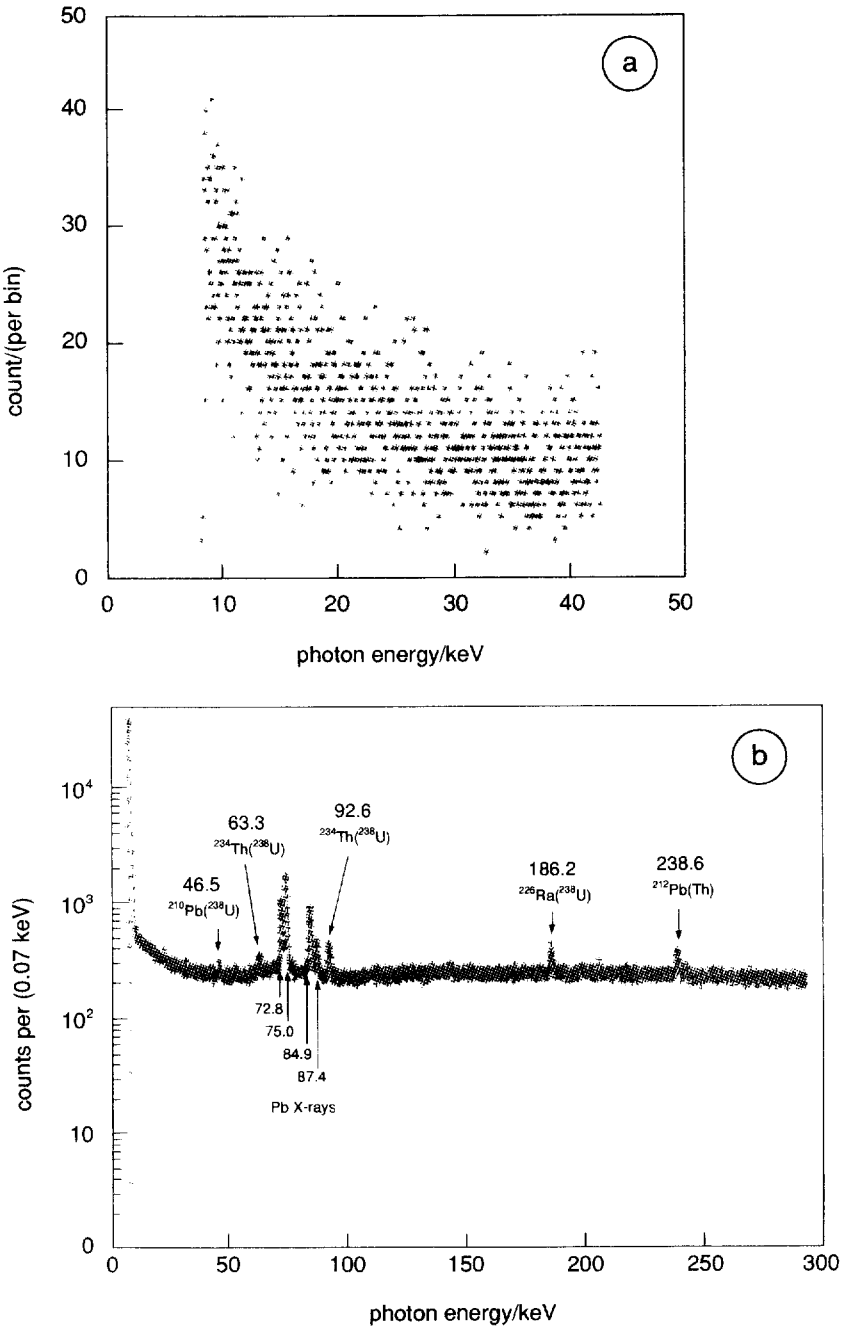


Fig. 1. Background spectra in the Pb cave. (a) Featureless region from 7 to 45 keV, for the Si(Li) X-ray detector; total count of 1.2×10^4; counting time of 361.2 h. (b) 0 to 300 keV region, with spectral peaks identified, for the HPGe detector; total count of 1.06×10^6; counting time of 275.6 h.

2.1. Background radiation-shielding

Background radiation was monitored continuously by a NaI(Tl) detector placed in a lead-shielded cave and intermittently by Ge and Si(Li) detectors in a separate lead-shielded cave when the electrolytic cell was not in operation. The two caves, located approximately 2.0 m from each other, were shielded by ca. 5 cm thick lead bricks. The Pb shielding reduced the background radiation, defined here as the spectrum recorded with the electrolytic cell in place but with no cell current, by a factor of twenty. Both detectors showed constant background over a period of several months. The γ- and X-ray detectors and the electrolytic cell remained in a fixed position during experimental runs. Examples of the background spectrum, recorded in the cave and covering regions from 7 to 40 keV and 15 to 300 keV are illustrated in Figs. 1a and 1b, respectively. It is seen that the region from 7 to 40 keV is featureless; in contrast, the region between 15 and 300 keV exhibits well defined peaks.

2.2. Radiation detection; X-, γ-rays

The procedure and data reduction are as follows: Signals from the p-type high purity Ge detector (HPGe-EG & G Ortec), with crystal dimensions of 5.8 cm diameter and 6.8 cm length, are amplified and analyzed by a Davidson portable multichannel analyzer using 4096 channels with a gain of either 30 or 300. Other features: the crystal has an absorbing layer of Al (1 mm) and inactive Ge (0.7 mm); the number of equivalent attenuation lengths equals 13, 1.9 and 0.6 at 20, 40 and 60 keV, respectively. The relative efficiency of the crystal is 37% at 1.33 MeV (defined as Ge efficiency/3 in. $\times$ 3 in. NaI(Tl) at 25 cm). The spectral data are recorded on minicassette tape and transferred to a work station for processing. Cell spectra which have equivalent calibration parameters are compared with the background spectrum on a bin-by-bin basis using the standard χ-square distributed test statistics. The signed square root of the test statistics for each bin is plotted in units of standard deviation as a function of bin energy. The procedures and data reduction for the continuous monitoring of background radiation by the NaI(Tl) detector (2 in. $\times$ 8 in. crystal coupled to RCA 8575 PMT) are as follows: PMT signals are amplified and analyzed with a Nuclear Data Portable MCA using 512 channels. Spectral data (50–1500 keV) are recorded on minicassette tape for further processing. Each data accumulation period count rate for the 75–1500 keV range is calculated and plotted. The intensity of the X-rays flux was measured with a Si(Li) detector, (Kevex model PSI-amplifier model 4561), placed in close proximity to the operating electrochemical cell.

2.3. Cell design

Three types of electrochemical cells were employed. The first type, shown in Fig. 2a, was designed to provide overall information on spectra up to ca. 3000 keV and to monitor the temperature of cell elements in order to observe, in a crude fashion, time dependent heat generation in the course of Pd/D codeposition and electrolysis of D_2O, respectively. For this purpose, the working electrode and the spirally wound Pt counter electrode were centrally located and the thermocouples attached accordingly.

In the second design, Fig. 2b, the working and counter electrode assembly was modified to provide an open structure of the counter electrode. A flat Pd foil, instead of a cylinder (cf. Fig. 2a) was used as the working electrode. The uniformity of the charging current was realized by maintaining a uniform distance between the electrodes. This design allowed us to record lower energy levels of the emitted X-rays by placing the whole electrode assembly within 0.5 to 0.7 cm of the X-ray detector's beryllium window. However, the increase in sensitivity was at the expense of temperature measurements; the latter was monitored in the electrolyte phase only.

Finally, to extend the detection capabilities to still lower intensities of the radiation flux and lower energy levels, the third design employing a cathode in the form of an open wire Ni mesh, onto which Pd is deposited, and placed in close proximity to a thin, ca. 0.03 mm wall cell made of Mylar, Fig. 2c, was introduced. The cell design differs from that used by Bennington et al. [2] or Ziegler et al. [7] in two ways: it assures a more uniform distribution of the charging current density and, because of the open structure of the working electrode and the close proximity to the detector, it substantially reduces the attenuation of X-rays while maintaining uniform current density.

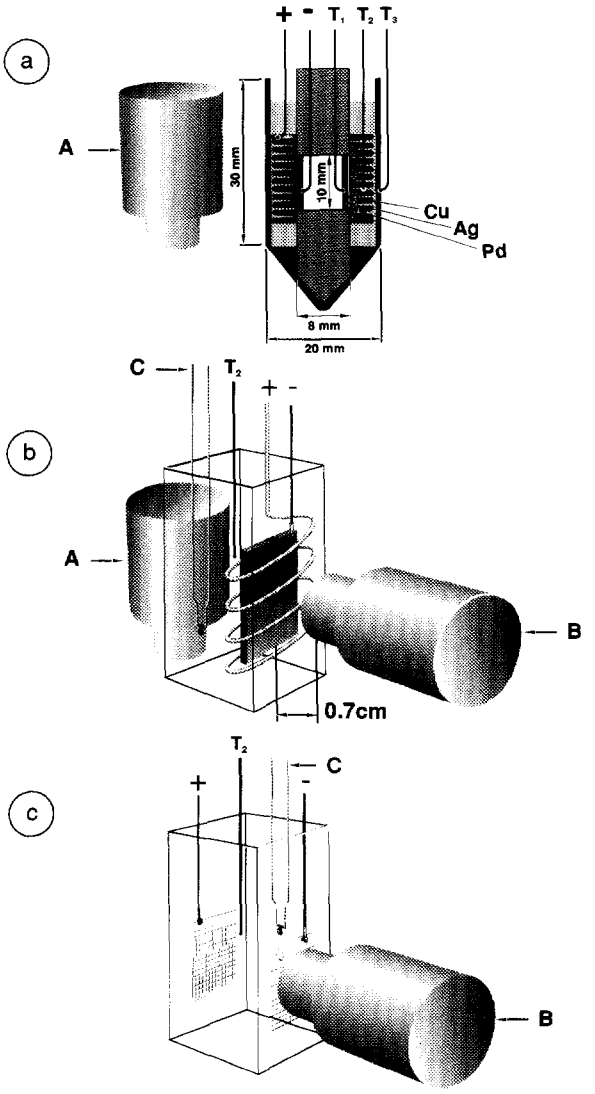


Fig. 2. Electrolytic cells. (A) γ-ray detector; (B) X-ray detector; (C) reference electrode; thermocouples: T_1 attached to the interior of the working electrode; T_2 immersed in the electrolyte; T_3 to measure the cell wall temperature. (a) Centrally located electrodes assembly; cell designed for examination of the spectral region 15–3000 keV. (b) Movable electrode assembly: closest approach of the working electrode to the detector window of 0.5 cm; cell designed for the spectral region 15–300 keV and provided with dual detection system. (c) Cell designed for detection of soft X-rays. The detector window is separated from the working electrode by the thickness of the Mylar sheet.

The cells were connected to a power source and operated under either potentiostatic or galvanostatic control (EG & G model 362). Only a limited set of calorimetric data could be secured in the cells designed for the detection of electromagnetic radiation. Of these designs, Figs. 2a–2c, the calorimetric data recorded for the cylindrical electrodes, Fig. 2a, are deemed to be more reliable than the designs employing mesh electrodes. The cell current, potential and temperature were recorded every 10 min.

3. Results

In what follows, we consider observations made on Pd electrodes prepared by (i) electrodeposition from an aqueous solution of $Pd(NH_3)_4Cl_2$ at low current densities (e.g., 200 μA cm^{-2}) for a period of ca. 20 h followed by codeposition from the D_2O-electrolyte for the spectral region 15–3000 keV; (ii) using commercially available Pd foil for the spectral region 15–300 keV; and (iii) codeposition of Pd/D from the $PdCl_2$–LiCl–D_2O solution for the spectral region 7–40 keV.

3.1. Spectral region: 15–3000 keV

The first set of experiments was designed to provide an overview of the electromagnetic spectrum associated with events occurring during the cathodic polarization of the Pd/D system. The effect of two charging techniques was examined, viz., charging by a codeposition process and by absorption of electrochemically generated deuterium. It is noted that these two techniques produce vastly different surface morphologies: in the first case, a dendritic surface is created [6] and in the second case, prolonged charging promotes the formation of surface fissures [8]. In both cases, the spectral region 15–3000 keV, after subtraction of background, was featureless. Examining the data in terms of counts per second, we note an overall $1.8 \pm 0.1\%$ increase in the count rate during cell operation, Figs. 3a and 3b. To determine that the observed increase in count rate is statistically significant and not due to random events, we employ the t-test [9] where t is given by

$$t = \frac{\bar{x}_1 - \bar{x}_2}{\sqrt{\sigma_1^2/n_1 + \sigma_2^2/n_2}}, \qquad (1)$$

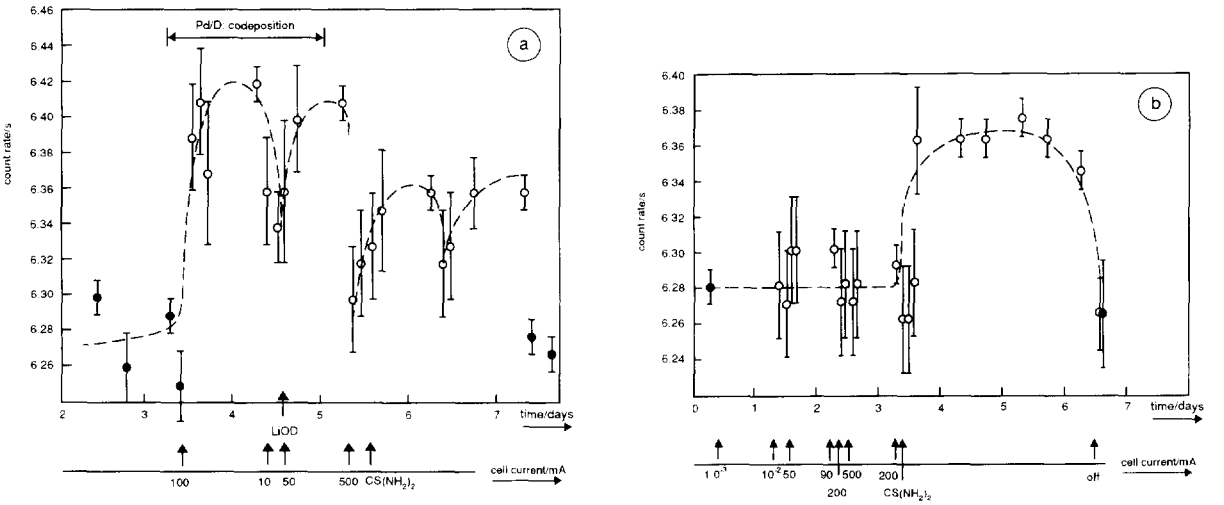


Fig. 3. Electromagnetic flux emitted during cathodic polarization of the Pd/D system; spectral region 15–3000 keV recorded by the Ge detector. Cell design as in Fig. 2a; electrode area of 2.51 cm^2 Ag deposited from a cyanide solution at 2 mA cm^{-2} for 10 min; the Pd layer is deposited from a $Pd(NH_3)_4Cl_2$–H_2O–LiCl solution at 200 μA cm^{-2} for 48 h; the cell current profile under galvanostatic control and electrolyte modifications is indicated; background – solid circles; operating cell – open circles. (a) Electrolyte: 0.003 M $PdCl_2$–0.3 M LiCl–D_2O LiOD added after depletion of Pd^{2+} ions (indicated by an arrow); addition of $CS(NH_2)_2$ is indicated by an arrow. Statistical information: background: $n = 6$, $\bar{x} = 6.272$, $\sigma = 0.019$; codeposition: $n = 9$ (the first 9 data points of cell operation); $\bar{x} = 6.383$, $\sigma = 0.027$, $t = 9.2$, $P(9.2) = 3.57 \times 10^{-20}$; $n = 9$ (the last 9 data points of cell operation); $\bar{x} = 6.336$, $\sigma = 0.023$, $t = 5.7$, $P(5.7) = 2.143 \times 10^{-8}$. (b) Electrolyte: 0.1 M LiOD; addition of $CS(NH_2)_2$ indicated. Statistical information: background and inactive period, first 9 data points of cell operation: $n = 11$; $\bar{x} = 6.285$, $\sigma = 0.016$; active period: $n = 11$, $\bar{x} = 6.322$, $\sigma = 0.048$, $t = 2.45$, $P(2.45) = 1.429 \times 10^{-2}$.

where $\bar{x}_1$ and $\bar{x}_2$ are the mean values for data sets consisting of n_1 and n_2 measurements, respectively, and σ_1 and σ_2 are the standard deviations of the means. The probability, $P(t)$, that increases with the count rate for n measurements are due to random events is very high for low values of t. However, that probability decreases rapidly with increasing t values (see Ref. [9], Table A VI.2). Here, we consider a t value greater than or equal to 3 ($P(3) = 2.699 \times 10^{-3}$) indicative that the difference between the means of the n_1 and n_2 data sets are statistically significant. The results of the statistical analyses are summarized in the figure captions.

While an increase in the count rate (ca. 4%) occurred shortly after the initiation of the Pd/D codeposition process on a dendritic surface, Fig. 3a, several days of charging were required to observe the same effect on a smooth surface, Fig. 3b. The common features for the two surface morphologies are: low level radiation as evidenced by the increase of the count rate and the effect of surface active agents, e.g., thiourea, on the initiation and/or re-activation of the X-ray producing process(es), Figs. 3b and 3a, respectively. As shown in Fig. 3a, the ca. 4% increase in the count rate terminated after the completion of the codeposition process (ca. 50 h). During the Pd/D codeposition, the count rate was not affected by the cell current profile and the emitted radiation, with $t = 9.2$, $P(9.2) = 3.57 \times 10^{-20}$, is accompanied by excess enthalpy production, as inferred from the higher temperature of the working electrode than that of the electrolyte phase. After completion of the codeposition process, a decrease in the count rate is observed. The addition of thiourea resulted in a statistically significant, $t = 5.6$, $P(5.6) = 2.143 \times 10^{-8}$, increase in count rate and the temperature of the bulk electrode exceeded the temperature of the electrolyte, clearly indicating the excess enthalpy production. Similarly, in Fig. 3b, an increase in count rate is observed with the addition of thiourea. Here, however, the statistics are weaker since $t = 2.45$, $P(2.45) = 1.429 \times 10^{-2}$. Nevertheless for $t = 2.45$, the probability that the increase in count rate is the result of random events is 1.4%.

3.2. Spectral region: 15–300 keV

Analyses of the 15–3000 keV spectral region indicate that the increase of the count rate occurs at low energy. Consequently, we redesigned the cell to reduce the attenuation of the radiation flux, Fig. 2b, and, additionally, we employed two independently operating detectors capable of viewing overlapping regions, viz., one for the X-ray and one for the γ-ray regions. Four experiments, each of ca. one month duration, showed the same characteristic features, namely a simultaneous increase of the count rate as observed by both detectors. In this set of experiments, a Pd foil was charged under controlled overpotential in the sulfate electrolyte with $BeSO_4$ as the additive. The results, summarized in Fig. 4, are as follows: No radiation above background is noted during the initial period of charging (ca. first eight days). The flux intensity varies with time as illustrated in the γ-ray count rate by the two periods of time I and II. Within these periods a statistically significant increase in the radiant flux, with $t = 8.69$, $P(8.69) = 3.31 \times 10^{-18}$ and $t = 14.89$, $P(14.89) < 10^{-23}$, respectively, has occurred. Examining the same periods of time for the X-ray component we note no increase in the count rate within the first region ($t = 0.44$, $P(0.44) = 3.3 \times 10^{-1}$). In contrast, region II reveals a statistically significant increase in the count rate, as evidenced by $t = 5.0$, $P(5.0) = 5.73 \times 10^{-7}$. The flux intensity exhibits a weak dependence on the overpotential (also cell current). Parenthetically, we observe upon subtraction of the background, no clearly discernible peaks within this spectral region.

3.3. Spectral region: 7–40 keV

The electrolytic cell shown in Fig. 2c was employed to examine the low energy spectral region, e.g., 7–40 keV. In all runs we observed an increase in the count rate especially in the low energy end. In some instances, as illustrated in Fig. 5, it appears that weak peaks are emerging, one at ca. 11 keV, point A, the other at ca. 20 keV, point B. The position of point B is unchanged while that of peak A tends to shift to lower energies without clearly defined changes in experimental conditions.

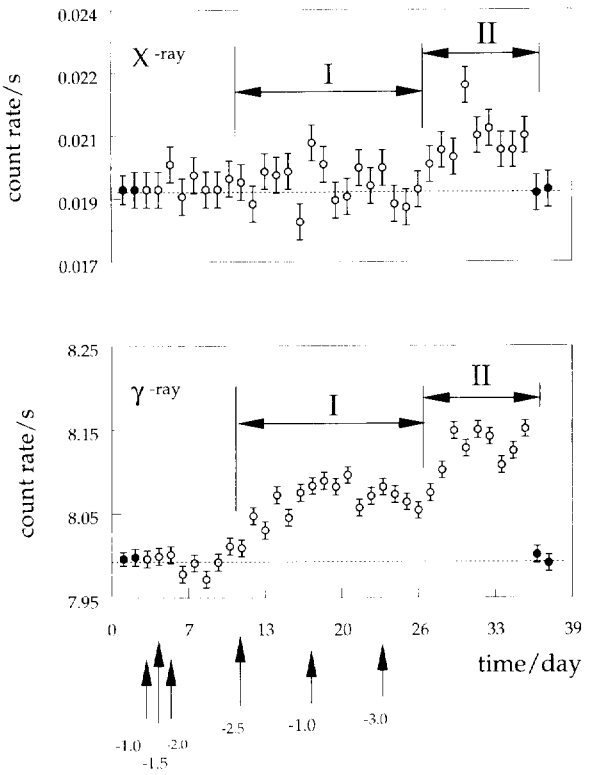


Fig. 4. Electromagnetic flux emitted during cathodic polarization of the Pd/D system; spectral region 0–300 keV: upper segment: spectral region 7–40 keV; lower segment: spectral region 40–300 keV. The arrows indicate the applied overpotential, in V, versus the Ag/AgCl reference electrode; background – solid circles; operating cell – open circles. The dashed line in both plots indicates background count rate. Cell design as in Fig. 2b; electrode: Pd foil, area 2 cm^2; electrolyte: 0.3 M Li_2SO_4–D_2O–Be (100 ppm added as $BeSO_4$). Statistical information of the 7–40 keV region: background: $n = 12$ (four background data points plus the first eight data points during cell operation), $\bar{x} = 0.0191$, $\sigma = 0.00026$; region I: $n = 16$, $\bar{x} = 0.01917$, $\sigma = 0.00057$, $t = 0.44$, $P(0.44) = 3.3 \times 10^{-1}$; region II: $n = 9$, $\bar{x} = 0.0204$, $\sigma = 0.00068$, $t = 5.00$, $P(5.00) = 5.73 \times 10^{-7}$. Statistical information of the 40–300 keV region: background: $n = 12$ (four background data points plus the first eight data points during cell operation), $\bar{x} = 7.994$, $\sigma = 0.006$; region I: $n = 16$, $\bar{x} = 8.057$, $\sigma = 0.030$, $t = 8.69$, $P(8.69) = 3.31 \times 10^{-18}$; region II: $n = 9$, $\bar{x} = 8.126$, $\sigma = 0.026$, $t = 14.89$, $P(14.89) < 10^{-23}$.

4. Discussion

The cell design employed in this research was selected to optimize the probability of detecting X-emissions during electrochemical loading of Pd. Si-

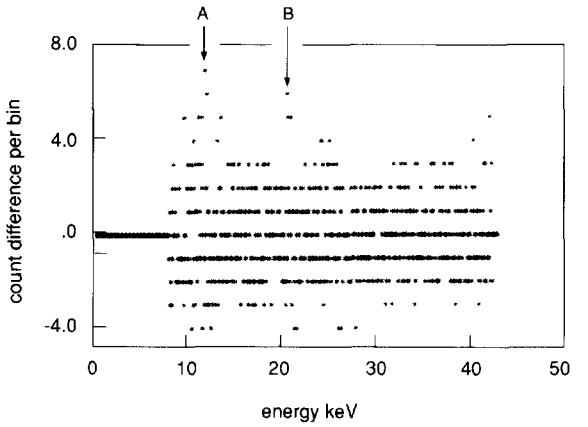


Fig. 5. X-ray spectrum emitted during cathodic polarization of the Pd/D system; spectral region 7–40 keV; background spectrum subtracted. Cell design as in Fig. 2c.

multaneous measurement of other possible markers, e.g., excess heat was not possible without disturbing the integrity of the experimental procedure. The results presented here represent a condensation of data collected over the course of two years and include experiments run under a variety of electrochemical conditions.

4.1. Methodology of measurements

Reliable analysis of low level radiation fluxes requires that the detectors and cell be shielded. However, even with shielding background radiation arises from cosmic rays interacting with the heavy atoms of the shielding material, e.g., Pb, cf. Fig. 1b. To insure an acceptable interpretation of weak signals, a continuous and independent monitoring of the background is needed, preferably by an instrument having higher sensitivity. For this purpose we selected the NaI(Tl) detector. In our experimental arrangement the background radiation, in identically shielded caves, was five times higher than when measured by the Ge detector. As indicated, vide Section 2.1, the background radiation was constant throughout the course of our experiments. To illustrate, the mean value of the background count rate from the NaI(Tl) detector for a six week period was 10.17 ± 0.04 cps while the values for each of the individual weeks was 10.144 ± 0.056, 10.147 ± 0.036, 10.185 ± 0.038, 10.174 ± 0.025, 10.134 ± 0.028, and 10.112 ± 0.030.

The argument usually offered for the rejection of the reported behavior of the polarized Pd/D system is that the low intensity of the radiant flux is, in reality, due to electrical noise. This argument is less compelling if a dual detection system is employed. Here, the dual system, consisting of the Si(Li) and Ge detectors, viewing simultaneously the electrochemical cell and operating independently from each other, exhibited the same behavior, i.e., a simultaneous increase of the count rate as illustrated in Fig. 4. While there is a general correspondence in the count rates between the X-ray and γ-ray detectors, i.e., the peak count rates for both detectors vary in the same manner, they exhibit different slopes. The γ-ray data in Fig. 4b appears to have two components: one which correlates with the X-ray data and another which corresponds to a monotonic increase in count rate. It is noteworthy that with termination of cell operation, the count rates observed by both detectors were as typical as that observed for background. Such behavior suggests a complex mechanism(s) responsible for the generation of the radiation.

4.2. Analysis

Several factors support the argument that the observed increases of the count rates can be attributed to electromagnetic emanation from the cell. First, as shown in Fig. 4, there is definite correspondence in count rates versus time between the X-ray and γ-ray detectors. Second, the additives, e.g., thiourea and Be^{2+} ions as well as the surface morphology, affect the intensity of the radiation flux, cf. Figs. 3 and 4. Third, the codeposition method of loading exhibited a shorter initiation time before the appearance of positive count rate deviations than the electrochemically charged electrodes; and finally, the increased count rates are observed sporadically, similar to other reported activities in these systems.

The low energy spectral distribution, cf. Fig. 5, reveals two features, viz., an increase of the count rate and the presence of rather weak peaks, one at ca. 20 keV and another at ca. 8–12 keV. This behavior is in general agreement with statements presented by other researchers. For example, Bennington et al. [2] stated: "any nuclear event depositing its energy within the Pd lattice will, in theory, produce X-rays by refilling of the K_α-shell of the excited Pd atoms". Buehler et

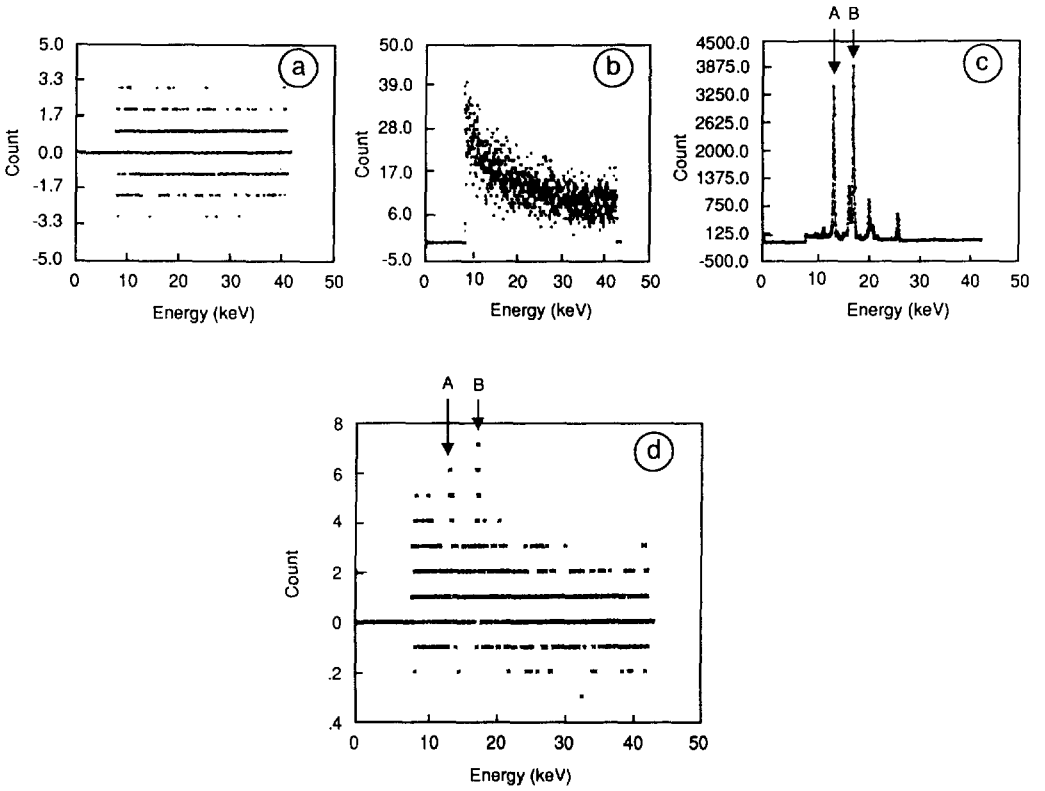


Fig. 6. Computer simulation of the addition (superposition) of weak spectral lines to the broad energy distribution (bremsstrahlung). (a) The difference of two background files illustrating a symmetric distribution about zero. (b) Energy distribution of the X-ray emanating from thorium oxide. (c) X-ray spectrum of Am: peak A: 13.76 keV L_{α_2}: $L_{III}M_{IV}$; peak B: 17.71 keV L_{β_1}: $L_{II}M_{IV}$. (d) Computer simulated energy distribution for a sum of: 0.0015 Am spectrum (cf. Fig. 6c); 0.02 ThO_2 spectrum (cf. Fig. 6b) and a difference of two separate backgrounds, all normalized to a 24 h period. Note: (i) asymmetry about zero due to bremsstrahlung; (ii) the emergence of weak Am peaks A and B.

al. [3] noted that charged particles, generated in the course of a nuclear event, e.g., p^+, t^+, α^{2+} particles, would ionize the Pd atoms to produce the K_α or K_β X-rays. On the other hand, because of the high density of oscillating plasma, a broad energy spectrum is expected [4,5,10].

We interpret the spectrum illustrated in Fig. 5, as resulting from the superposition of a weak peak upon a featureless background, e.g., the sharp peak of Pd K_α superimposed upon the bremsstrahlung arising from the oscillating plasma of the cathodically polarized Pd/D system. To demonstrate this we proceed as follows: First, as expected, the subtraction of two backgrounds recorded by the same arrangement within two time periods, is symmetrical around zero, Fig. 6a. Second, we constructed a model spectrum which contained a simulated bremsstrahlung component and a discreet line source component to determine the appearance of the resulting composite. To simulate the bremsstrahlung, we recorded the thorium oxide spectrum, Fig. 6b, while the americium spectrum was selected to represent the contribution of a line source, i.e. sharp peak(s), Fig. 6c. Addition of these spectra and the subtraction of the background resulted in the spectrum in Fig. 6d. The spectrum in Fig. 6d exhibits a structure very much like the experimental spectrum presented in Fig. 5. While this is not definitive evidence that Fig. 5 is a composite, it at least demonstrates that a spectrum consisting of a few energy peaks superimposed on a bremsstrahlung background is a con-

sistent interpretation of the observed spectrum shown in Fig. 5. Based on this interpretation, the emerging point B, Fig. 5, is most likely the Pd K_α peak. The assignment of peak A is less certain. Employing the approximate formula relating the energy of the K series to the number of protons, Z, viz., $Ry(Z-1)^2$; Ry = 13.5 eV gives for the 11–12 keV energy range the value of Z = 28–30. One of the elements having the required number of protons is nickel, used here as the substrate onto which the Pd/D system was deposited. However, the known energy of the Ni K series is substantially less than that observed here. We cannot rule out the possibility that peak A is due to Pt, which is a cell component (our anode) and has L line emissions in the 10–13 keV range. It is possible that during prolonged electrolysis in Cl^- solutions, small amounts of Pt could be transported from the anode to the cathode.

With respect to the effect of additives on radiation emission processes, both Be^{+2} and thiourea are known to increase the rate and degree of deuterium uptake. Similarly, radiation emissions are observed with extended surfaces, such as the globular or dendritic growths associated with Pd/D codeposition, which increase deuterium uptake. Collectively, these observations provide evidence for a coupling between deuterium uptake and radiation emissions.

5. Conclusions

Accepting the conclusion that weak electromagnetic radiation is responsible for the observed results, we make the following statements:

(i) While attempting to monitor the emanation of X-rays from the cathodically polarized Pd/D system, an adequate shielding must be provided and the working electrode must be placed close to the detector window.

(ii) The cathodically polarized Pd/D system emits X-rays with a broad energy distribution and with an occasional emergence of recognizable peaks. Because of the low intensity of the electromagnetic flux, its detection requires that cells be constructed accordingly.

(iii) The emission of X-rays appears to be sporadic and of limited duration.

(iv) Surface morphology influences radiation emissions – codeposited Pd/D electrodes exhibit shorter initiation times prior to the observation of radiation emissions. In the cases when either Be^{2+} ions or thiourea were added to the electrolyte, similar positive effects were observed.

Acknowledgement

The authors would like to thank Dr. Frank Gordon for his enthusiastic support. We would also like to thank the referees for suggesting that the line between 10 and 13 keV may be attributed to the Pt L lines.

References

[1] M. Fleischmann and S. Pons, J. Electroanal. Chem. 261 (1989) 301.
[2] S.M. Bennington, R.S. Sokhi, P.R. Stonadge, D.K. Ross, M.J. Benham, T.D. Beynon, P. Whithey, I.R. Harris and J.P.G. Farr, Electrochim. Acta 34 (1989) 1323.
[3] D.B. Buehler, L.D. Hansen, S.E. Jones and L.B. Rees, Is reported "excess heat" due to nuclear reactions?, in: Frontiers of cold fusion (Universal Academy Press, Tokyo, 1993) p. 245.
[4] Y. Kucherov, A. Karabut and I. Savvatimova, Heat release and product yield of nuclear reactions in Pd–D systems, in: Fourth ICCF, December 1993, Lahaina, Hawaii.
[5] J.P. Vigier, New hydrogen energies in specially structured dense media: Capillary chemistry and capillary fusion, in: Frontiers of cold fusion (Universal Academy Press, Tokyo, 1993) p. 409.
[6] S. Szpak, P.A. Mosier-Boss and J.J. Smith, J. Electroanal. Chem. 302 (1991) 255.
[7] J.F. Ziegler, T.H. Zabel, J.J. Cuomo, V.A. Brusic, G.S. Cargill, E.J. O'Sullivan and A.D. Marwick, Phys. Rev. Lett. 62 (1989) 2929.
[8] D.R. Rolison, W.E. O'Grady, R.J. Doyle and P.P. Trzaskoma, Anomalies in the surface analysis of deuterated palladium, in: Proc. First Annual Conf. on Cold fusion, Salt Lake City, UT, p. 272.
[9] S.L. Meyer, Data analysis for scientists and engineers (Wiley, New York, 1975).
[10] R. Antanasijevic, I. Lakicevic, Z. Maric, D. Zevic, A. Zaric and J.P. Vigier, Phys. Lett. A 180 (1993) 25.